Isolator flow response to Scramjet-Ramjet Transition in a Scramjet Engine

Rajarshi Das, Ha Jeong Ho and Heuy Dong Kim
das2010andong@gmail.com
Andong National University
Department of Mechanical Engineering
Andong
Republic of Korea

Foluso Ladeinde
Stonybrook University
Department of Mechanical Engineering
Inchon
Republic of Korea

ABSTRACT

Combustor-Isolator interactions during scram to ram mode transition in a hydrogen-fueled scramjet combustor are numerically investigated at an operating Mach number of M=2.17. The two- dimensional flow domain is modeled based on the isolator and combustor sections of a dual-mode combustor setup. The associated thermal choking downstream of the injector and its impact on flow properties at the exit of the isolator is also investigated. It is observed that the scram to ram mode transition is a function of the inlet total temperature and the fuel air equivalence ratio. Supersonic core flow area at the exit of the isolator decreases as the equivalence ratio increases during the scram mode of operation of the engine. The obtained results also showed a region of in-operability of the dual-mode engine as the mode transition takes place. Apart from this, strong aero-thermodynamic effects triggering transition is observed from the results. Numerically obtained results are in good agreement with theoretically predicted values.

Keywords: Dual mode combustor; transition; region of inoperability

NOMENCLATURE

A   area

D   depth of cavity

H   height of the flow domain

k   turbulent kinetic energy

L   length of cavity

M   Mach number

$\dot{m}$ mass flow

P   pressure, kPa

T   temperature, K

t   flow time

x   distance along the combustor axis

Y   perpendicular distance along the combustor axis from bottom wall

cav   cavity

in   inlet

x_c location of thermal choking along axial direction

Symbols

φ fuel-air equivalence ratio

∞ freestream/ boundary layer edge location

ρ density

0   stagnation conditions

1   isolator inlet

2   isolator exit

1.0   INTRODUCTION

Dual mode scramjet combustors are designed to operate efficiently at both low and high supersonic Mach numbers. At lower M_∞, the engine is supposed to operate at subsonic speeds or in the ramjet mode. At $M_\infty = 6$ or higher, the operating mode of the combustor should change to scramjet mode to avoid the undesired total pressure loss associated with diffusing the airflow to subsonic velocities within the combustor [1]. Rapid increase of pressure inside the combustor takes place as combustion commences. This increase in pressure at times surpasses the level that the boundary layer can support. At this juncture, the boundary layer separates and a pre-combustion shock train is formed upstream of the fuel injection location. To avoid any interaction of this shock system with the air intake region of the propulsion system, a long constant cross section duct is placed between the inlet and the combustor which is termed as the isolator. This helps in stabilizing and accommodating the shock train. Interaction of the flow through the isolator and the physical changes occurring inside the combustor is an important aspect of dual mode combustor design.

During the past two decades, investigators have assessed the performance of the various components of a dual mode combustor individually. To replicate downstream pressure rise due to combustion, valves have been used by some researchers [2-4]. The unsteady flamefront and other combustion parameters have been studied using several injection and mixing techniques widely [5-8]. Response of the shock train inside the isolator during thermally choked and unchoked downstream conditions has also been investigated [9-11]. However, experimental investigation into such processes is challenging to undertake. Hence, recently, investigators have shifted to numerical simulations of the supersonic combustion phenomena with the powerful computers and robust numerical algorithms available today. Researchers have numerically investigated such flows using various models which has created a substantial database for comparative study of the solutions obtained [17-19]. However, despite many years of research, large number of issues related to description of supersonic turbulent reactive flows still remains unanswered.

Several of the unanswered questions are related to the changes in the flow field occurring when transition takes place. As the downstream flow changes from thermally unchoked to choked conditions, response of flow properties in the isolator region to such conditions is a major area that has remained sparsely reported in available literature. The flow condition limiting properties for scram-ram transition also needs proper defining for the development of scramjet engines. Recently, Fotia and Driscoll [20] reported such investigation, but much of their results are dependent on theoretical analysis under constrained conditions. This current study is an attempt to remove some of these constraints and present the results under more realistic conditions. Also through this presentation an attempt has been made to highlight some flow field features that are usually challenging to capture using experimental techniques.

2.0   TEST SETUP

The two-dimensional flow domain is modeled based on the isolator and combustor section of a dual mode combustor setup. The domain consists of a 358mm long constant cross section isolator connected directly to a 444.3mm long combustor section. Direct cross flow fuel injection takes place from the floor through a 2.2mm wide injector mounted at the end of the isolator section as is shown in Figure 1. The injector actually demarcates the end of the isolator and the start of the combustion chamber. A trailing edge wall ramp cavity of L/D ratio of 4 acts as the flame-holder with pilot fuel injected through a 0.5mm wide injector located at the floor and trailing edge wall of the cavity. The cavity is followed by a 4° divergent bottom wall which exhausts the combusted flow into atmospheric conditions. Vitiated air enters the constant area isolator at elevated total temperatures (T_0) of 1000K and 1200K at M =2.17. The inlet total pressure, P_0 has been maintained as 448.2kPa. The analysis is carried out at different equivalence ratios [φ] ranging from $\varphi=0.13$ to $\varphi=0.25$. A $\varphi=0.0$ (no injection) case is also numerically investigated considering steady flow conditions. This served as the initial instant for the injection cases.
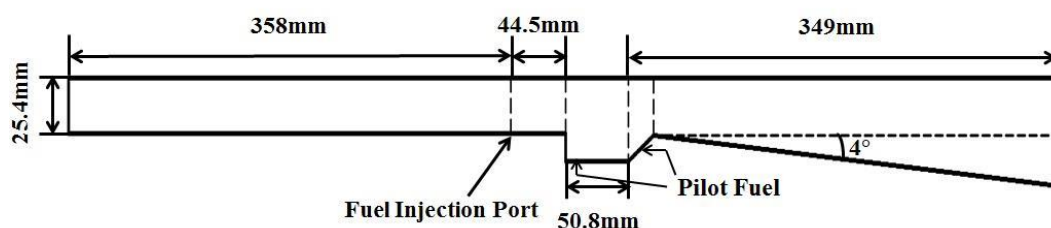

Figure 1 Schematic of test domain

Unsteady calculations are conducted initializing from this case with increasing φ from 0.13 to 0.25. Hydrogen is used as both the main and the pilot fuel. To maintain the equivalence ratio, the total injected fuel mass is divided between the main injector and the pilot injector. 88% fuel is injected through the main injector and the rest is injected through the 2 pilot injectors in equal proportions. Earlier, Micka and Driscoll [21] observed that increasing m_{cav}/m_{in} lowered the combustor lean ignition limit. According to this study, between m_{cav}/m_{in} =0.07 and 0.21, the ignition limit change in terms of φ remains almost same. The fuel injection conditions have been maintained at a constant $T_0 = 288K$ and varying total pressure $P_0 = 690kPa \sim 1090kPa$ depending on the equivalence ratio. Under these criteria, the injector operated at choked conditions. The flame holder region has been patched with a high temperature zone to replicate a spark to ignite the pilot fuel.

3.0   NUMERICAL PROCEDURE

The flowfield inside the test section is numerically simulated using commercially available software ANSYS v 15.0. Two dimensional, unsteady density based Navier Stokes scheme is applied for the solution combined with the species transport model. The coupled formulation of density based solver was used for its applicability in compressible high Mach number flows. Wilcox's k-ω turbulence model is used for modeling the flow field turbulence as it predicts the near wall behavior better than the other models and also predicts the mole fraction of species approximately similar to experimentally obtained values [22]. A single step finite rate chemistry following reversible reaction between fuel and oxidizer is used to model the chemical interaction between fuel and air. Connaire et al. [23] observed that with addition of turbulence-chemistry interaction, there is dramatic increase in the turbulent diffusivity throughout the flame region and different chemical schemes do not alter the mixing and combustion process significantly. Through the species transport model, reactions were defined as volumetric with full multicomponent, inlet and thermal diffusion. Also, inlet air is described to constitute 0.79% nitrogen and 0.21% oxygen through the species transport model. This oxygen serves as the oxidizer for the fuel injected. Even under vitiated conditions, the mass fraction of oxygen and nitrogen was kept as the same under ordinary conditions which replicates supply of excess oxygen at the inlet during actual experiments [24]. Spatial discretization was achieved by second order upwind scheme.

The test section model was created using GAMBIT where the mesh was clustered near to the wall so that the viscous effects are properly resolved during the simulation. The flow domain was partitioned into 1.06 million mesh elements. A blow up of the meshed model is shown in Figure 2. Finely structured mesh was created in the region adjacent to the cavity and injector to resolve the density gradients occurring due to presence of shock and thermal transients. The minimum grid spacing adjacent to the wall of the flow channel was kept at 0.001mm which maintained a proper wall y+ value (y+ ~1).
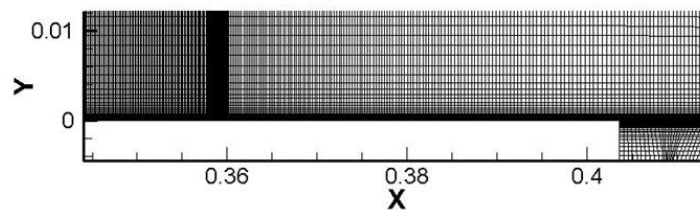

Figure 2 Finely meshed domain adjacent to wall and main injector

Pressure inlet and pressure outlet condition was specified at the inlet and exit respectively. For the unsteady simulation of the combustion cases, a time step of $\Delta t=10^{-8}$ s was implemented for the transient formulation and the numerical scheme was run with increasing φ. The solution was allowed to stabilize and converge after which a small increment in φ of 0.01 was given for the next case. This procedure was followed till the value of φ increased to 0.25. For every case the mass flow imbalance between the inlet, outlet, main and pilot injectors was allowed to fall below the order of 10^{-3}, before increasing the equivalence ratio.

3.1   Validation of numerical procedure

In similar lines of other numerical investigations, grid independence study, different turbulence models and multiple analyses under same flow field conditions were conducted to converge into reliable calculation results using the numerical tool. As a validation case, the quantitative aspects of the flowfield in terms of isolator inlet and exit flow properties and the supersonic flow region at the exit of the isolator is described and discussed in this section. From the converged numerical solutions at $\varphi = 0.15$ and $\varphi = 0.22$ at an inlet T_0 of 1000K, the static pressure at discrete points along the bottom wall of the combustor setup is plotted and shown in Figure 3. This plot shows the normalized static pressure distribution along the bottom wall under the scramjet

and ramjet mode of the engine operation. The experimental values of static pressure obtained during experiments by Fotia and Driscoll [20] are also plotted along with the numerically calculated values obtained during the course of this investigation. The numerical results agree well with that of the experiment. Plotting the pressure data obtained over the bottom wall as shown in Figure 3 also serves as an exercise to verify the robustness of the numerical approach adopted for this study.
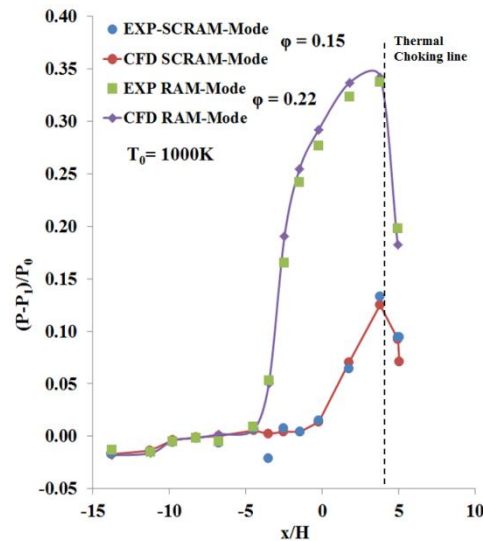

Figure 3 Pressure variation along the combustor wall under the 2 operating modes

Operating in scramjet mode, the rise in static pressure along the wall is observed to be located aft of the injector. The location value of x/H=0 indicates the injector location at the exit of the isolator. Functioning in the ramjet mode, the static pressure is observed to increase suddenly considerably ahead of the injector location due to the presence of the normal shock generated in the flow field. The location of the thermal choking point is also plotted in this figure which is theoretically calculated under frictionless, zero mass addition conditions as described by Shapiro [25] for a diverging duct by the following equation-

$$\frac{1}{A}\frac{dA}{dx_c} = \frac{1+\gamma}{2}\frac{1}{T_0}\frac{dT_0}{dx_c} \qquad \dots (1)$$

where, the gradient of T_0 is determined by the heat release during combustion.

Between the ram and the scram mode, the pressure in the isolator section rises abruptly, indicating the presence of a pseudo-shock while operating in ram mode. This pseudo-shock is generated due to the thermally choked downstream conditions during ram mode. As the φ was increased in steps, it was observed that the thermal choking conditions suddenly occur at φ=0.19 downstream of the injection location. This is observed from the Mach number contours displayed in Figure 3 for φ=0.2.

4.0   RESULTS AND DISCUSSION

The flow field inside the model combustor is analyzed in terms of pressure, Mach number and temperature distribution and the supersonic flow regions in the flow domain. The variations of pressure in the flow field translate as the shock structure in the flow domain. The Mach number variation in the flow field provides information on mode transition and the temperature distribution helps distinguish the flame front in the domain. The results of these analyses are presented in this section.

The Mach number variation in the flow domain for an inlet T_0 of 1200K is shown in Figure 4 as the equivalence ratio is varied from φ=0.0 (no injection) to φ=0.25. The change in the M distribution indicates that the flow field changes from the scram to ram mode as the equivalence ratio is increased. At φ=0.0, the flow inside both the isolator and the combustor is fully supersonic with a shock wave observed at the trailing edge of the cavity. This is due to the movement of the shear layer over the cavity. The shear layer is visible over the cavity in Figure 4. At φ=0.13, a weak shock wave is observed upstream of the injection location at x=0.358m and the flow aft of this shock wave is observed to be locally supersonic. As the equivalence ratio is changed to φ=0.17, this shock wave becomes stronger and is positioned at the same location as that of when φ=0.13. The flow aft of the shock wave is observed to slow down. On increasing φ to 0.2, the shock wave become much stronger as is observed from its wave angle and the downstream flow field. It is also observed to move upstream much ahead of the injection location and positions itself at a site where x=0.345m. On further increasing φ, at

φ=0.25 the flow velocity upstream of the injector is observed to change into low subsonic speeds thereby indicating the onset of ram mode inside the combustor setup. This transition can be attributed to the coupled effect of the aeromechanical blockage generated by the injected fuel and the increase in downstream pressure due to combustion.
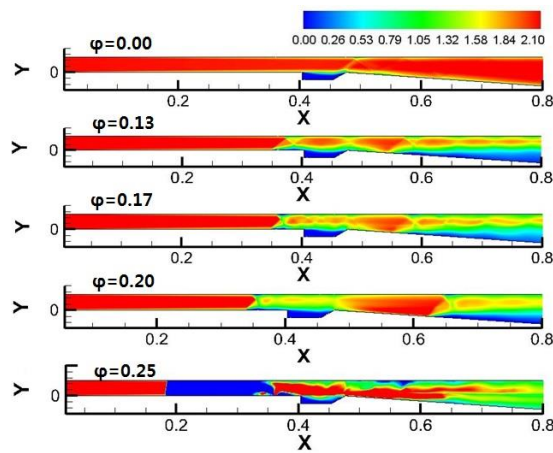

Figure 4 Mach variations in the flow domain at different φ

Based on the different inlet T_0 and φ used for the various cases, the two modes of operation of the supersonic combustor can be shown as is illustrated in Figure 5. The ram mode and scram mode operations are demarcated as function of the inlet T_0 and φ in this plot. The Fotia and Driscoll [20] transition line and the choked Rayleigh line is also plotted in this figure. It is observed that when the inlet T_0 is higher, transition occurs at a higher φ. At T_0 = 1000K, transition from scram to ram mode is observed to occur at φ>0.17 and for an inlet T_0 = 1200K, transition takes place at φ>0.19.
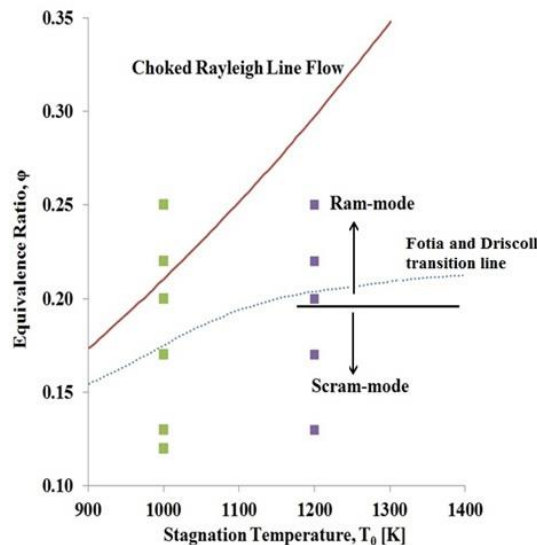

Figure 5 Combustion regimes as function of T_0 and φ

Mode transition occurs in the dual mode engine as the fuel-air equivalence ratio is increased as is shown in Figure 4. The response of the isolator flow during transition is investigated in detail based on the time dependent variation of the flow field structure in the flow domain. During this study, the events triggering the mode change is observed to be mostly based on the characteristics of the flow field boundary layer. This phenomena is discussed in detail in this section for an inlet operating temperature of T_0=1000K and φ=0.17. The sequential occurrence of events in the vicinity of the isolator exit is shown in Figure 6 based on the streamtraces in the flow domain. For this reason, flow at the inlet of the isolator is defined by 50 equally spaced streamtraces along the channel height. The number of streamtraces is decided based on the clarity provided in the images produced. The first image shown in Figure 6 is assumed to correspond to a flow time t=0.0ms. The flow time mentioned in the successive images is an estimate of the time lag between that image and the first one. At t=0.0, the flow is observed to be mostly undisturbed at the exit of the isolator at a location x=0.358m. The slight distortion is chiefly due to the injection and the associated weak shock wave at this location. Downstream,

above the cavity, the flow is observed to get compressed. As the pressure inside the cavity increases due to combustion, the free shear layer spanning the length of the cavity is forced out into the freestream. This compresses the flow above the cavity. In the next image at t=2.1ms this compression is observed to be more pronounced and the flow above the cavity gets constricted. The incoming boundary layer upstream of the cavity is also observed to get separated in this image. This is due to the adverse pressure gradient generated due to combustion downstream. More distortion of the flow field and full separation of the boundary layer upstream of the cavity are observed at t=2.56ms. The freestream flow is observed to be constricted through an imaginary throat like structure due to the high pressure generated in the cavity. Generation of this throat is purely due to aero-thermodynamic effects.
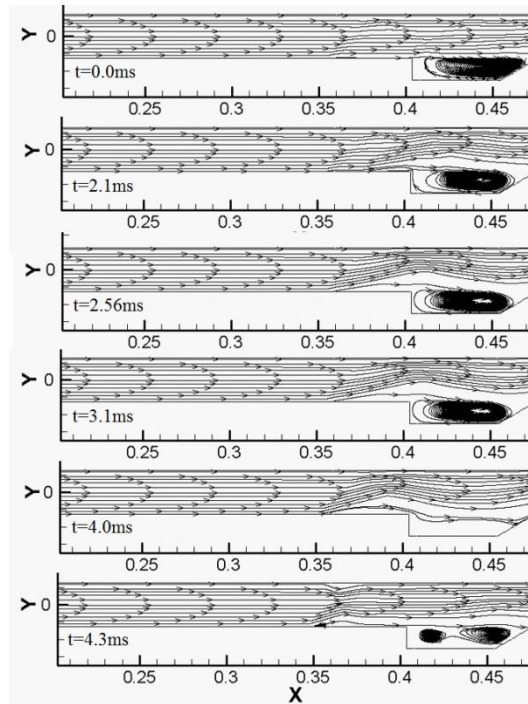

Figure 6 Boundary layer separation and generation of aerodynamic throat

Due to the adverse pressure, boundary layer separation is observed to surge upstream and the supersonic flow gets compressed as is observed at t=3.1ms. The imaginary throat also moves upstream towards the exit of the isolator and decreases in width. At t=4ms, as the shear layer dives back into the cavity, the separated boundary layer starts reattaching, downstream of the isolator exit. The separated boundary layer generates a strong shock wave as is observed from the Mach number distribution in the flow channel at $\varphi=0.17$ displayed in Figure 4. With the onset of this aero-thermodynamic throat, the incoming supersonic flow decelerates due to aerodynamic effects as it passes through the throat. As the width of the throat decreases, at some instant of time the flow downstream of the throat becomes subsonic and the ramjet mode of operation of the engine sets in. In Figure 4 localized subsonic flow immediately aft of the shock wave can be observed. Finally, at t=4.3ms, the imaginary aero-thermodynamic throat is positioned at the exit of the isolator (x=0.358m) along with a strong shock through which the flow diffuses to subsonic velocities during the ram-mode operation. Summing up, the adverse pressure gradient causes the boundary layer to separate which in turn generates the strong shock wave and the aero-thermodynamic throat through which the supersonic flow diffuses to subsonic velocities within a time period of approximately 2ms.

In Figure 6, at t=4.3ms, the boundary layer is observed to separate from the top wall also at the isolator exit. This may be due to the formation of a lambda shock at this wall as is observed in Fig.3 for $\varphi=0.17$. The turbulent boundary layer along the top wall may have separated ahead of the shock due to the adverse pressure gradient which triggered the lambda shock structure. However, this phenomenon is not probed in details during the course of this investigation.

Mach number distribution at the exit of the isolator plane (x=0.358m) during the transition process is studied in details. The mass flow averaged Mach number distribution at different times is shown in Figure 7. The exit plane is divided into 100 discrete points for this study and data was collected at all these locations at different time instances. The initial time instant is considered as t=0.0 as described in the previous section. The subsequent time instances are the delay time recorded post t=0.0ms. From Figure 7 it is observed that the transition phenomenon starts with the onset of the boundary layer separating from both the bottom and top wall

of the flow domain. The Mach number adjacent to the walls decreases due to separation of the boundary layer. The complex lambda shock structure results in the flow M to fall below sonic values in the middle of the channel at t=3.8ms. However, even during and post transition, the M is observed to be locally supersonic at some locations at the isolator exit. The average M at the isolator exit plane was calculated from the data collected at the different time instances. It was observed from the calculations that the average exit plane M suddenly drops from M=1.3 at t=3.8ms to M=0.9 at t=4.0ms. This sudden change of the average M at the isolator exit is further studied with reference to Heiser and Pratt's [26] theoretical analysis model in the following section.
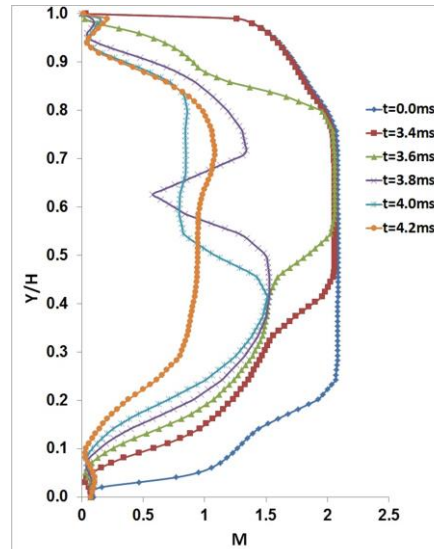

Figure 7 Mach number distributions at isolator exit plane

Heiser and Pratt [26] formulated a relation to determine the pressure recovered across the isolator as a function of M_2 and isolator inlet conditions. It assumes that the isolator flow is comprised of central supersonic core flow containing the shock train and the surrounding boundary layer at the edges. The equation that was developed based on conservation of mass and momentum in this core flow and the boundary layer region is –

$$\frac{P_2}{P_1} = 1 + \gamma M_1^2 - \gamma M_1 M_2 \sqrt{\frac{1+\frac{\gamma-1}{2}M_1^2}{1+\frac{\gamma-1}{2}M_2^2}} \qquad \ldots (2)$$

M_2 in the above equation is determined from the equations relating the area change and the stagnation temperature increase to the variation in Mach number. Theoretically, P_2 is then determined using this value of M_2. An overall theoretical assessment of the flow field inside the isolator was provided by Heiser and Pratt [26] when they expressed the effective core supersonic flow area at the isolator exit as –

$$\frac{A_{2c}}{A_1} = \frac{1}{\gamma M_2^2}\left[\frac{P_1}{P_2}\left(1 + \gamma M_1^2\right) - 1\right] \qquad \ldots (3)$$

This relation combined with Eqn. 2 provides a parabolic relationship between the pressure rise in the isolator and the supersonic core area contraction ratio as a function of the isolator inlet conditions. Using these equations, the theoretical relation between A_{2c}/A_1 and P_2 is plotted and shown in Figure 8 for inlet $T_0=1000K$. Some of the numerically calculated average M values are also plotted along with the theoretical variation.
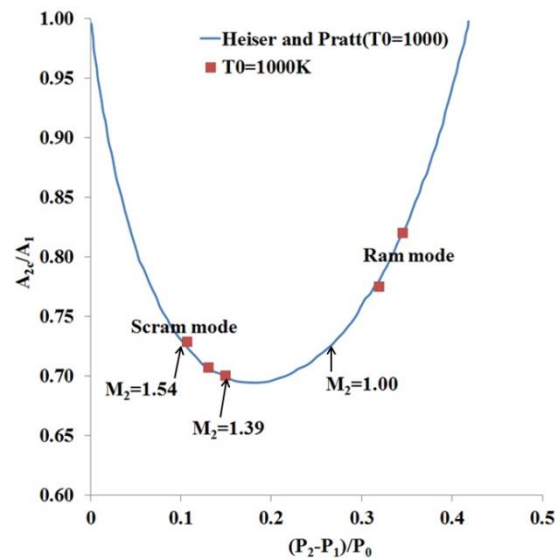
Figure8 $P_2 - A_{2c} - M_2$ dependence at T_0=1000K

The discrete numerical values shown in Figure 8 correspond to varying φ used for the study. The φ rise is synonymous with the increase of P_2 values along the horizontal axis of the plot. With increasing equivalence ratio, the supersonic core flow area at the exit of the isolator decreases and the static pressure P_2 rises. A decrease in M_2 is also observed as the equivalence ratio rises. As is observed from the plot, the regions of scram mode operation and ram mode operation is distinctly divided with region where the engine is inoperable. This region lies between $M_2 = 1.3$ to $M_2 = 1.0$ according to previous researchers [20].

5.0   CONCLUSION

The transition of operation of a scramjet engine from the scram to ram mode is investigated for a model scramjet engine at an operational M = 2.17. The response of the flow in the isolator to the transition is also investigated. It is observed that the transition is inter-dependent on the inlet T_0 and the fuel air equivalence ratio, φ. At higher T_0, the transition takes place at higher values of φ, thereby indicating more fuel consumption for the engine for mode transition to occur. Abrupt changes of flow properties are observed during change over from scram to ram mode with the results clearly showing a region of in-operability for the scramjet engine. Analysis of flow properties at the isolator exit shows that as the equivalence ratio increases, the static pressure increases with a decrease in flow M. The supersonic core flow area at the isolator exit decreases with increase in φ during the scramjet mode of operation. Deceleration of supersonic flow to subsonic velocities during mode transition occurs through an imaginary aero-thermodynamic throat generated due to boundary layer separation.

ACKNOWLEDGEMENT

REFERENCES

[1] CURRAN, E. T., LEINGANG, J. L., AND DONALDSON, W. A., "Review of High Speed Air Breathing Propulsion Systems," *Proceedings of the Eighth International Symposium on Air Breathing Engines*, AIAA, Washington, DC, June 1987.

[2] CARROLL, B. F., AND DUTTON, J. C., "Turbulence Phenomena in a Multiple Normal Shock Wave/Turbulent Boundary-Layer Interaction," *AIAA Journal*, Vol. 30, No. 1, 1992, pp. 43–48.

[3] OM, D., VIEGAS, J. R., AND CHILDS, M. E., "Transonic Shock-Wave/ Turbulent Boundary-Layer Interaction

in a Circular Duct," *AIAA Journal*, Vol. 23, No. 5, 1985, pp. 707–714.

[4] Carroll, B. F., and Dutton, J. C., "Multiple Shock Wave/Turbulent Boundary-Layer Interactions," *Journal of Propulsion and Power*, Vol. 8, No. 2, 1992, pp. 441–448.

[5] Hasselbrink, E. F., and Mungal, M. G., "Transverse Jets and Jet Flames. Part 2.Velocity and OH Field Imaging," *Journal of Fluid Mechanics*, Vol. 443, 2001, pp. 27–68.

[6] Micka, D. J., and Driscoll, J. F., "Stratified Jet Flames in a Heated (1390 K) Air Cross-Flow with Autoignition," *Combustion and Flame*, Vol. 159, No. 3, 2012, pp. 1205–1214.

[7] Rieker, G. B., Jeffries, J. B., Hanson, R. K., Mathur, T., Gruber, M. R., and Carter, C. D., "Diode Laser-Based Detection of Combustor Instabilities with Application to a Scramjet Engine," *Proceedings of the Combustion Institute*, Vol. 32, No. 1, 2009, pp. 831–838.

[8] Hasselbrink, E. F., and Mungal, M. G., "Transverse Jets and Jet Flames. Part 1. Scaling Laws for Strong Transverse Jets," *Journal of Fluid Mechanics*, Vol. 443, 2001, pp. 1–25.

[9] Goyne, C. P., McDaniel, J. C., Quagliaroli, T. M., Krauss, R. H., and Day, S. W., "Dual-Mode Combustion of Hydrogen in a Mach 5, Continuous-Flow Facility," *Journal of Propulsion and Power*, Vol. 17, No. 6, 2001, pp. 1313–1318.

[10] Rocci Denis, S., and Kau, H.-P., "Experimental Study on Transition Between Ramjet and Scramjet Modes in a Dual-Mode Combustor," *12th AIAA International Space Planes and Hypersonic Systems and Technologies Conference*, AIAA Paper No. 2003-7048, 2003.

[11] Kanda, T., Chinzei, N., Kudo, K., Murakami, A., and Hiraiwa, T., "Auto-ignited Combustion Testing in a Water-Cooled Scramjet Combustor," *Journal of Propulsion and Power*, Vol. 20, No. 4, 2004, pp. 657–664.

[17] Kim, S.W. and Jensen, T.J.; "Fluid Flow of a Row of Jets in Crossflow- A Numerical Study," *AIAA Journal,* Vol. 31, No. 5, 1993, pp. 806-811.

[18] Jachimowski, C.J.; "An Analytical Study of the Hydrogen-air Reaction Mechanism with Application to Scramjet Combustion," *NASA Technical paper* - 2781, 1988.

[19] Alexopoulos, G.A. and Hassan, H.A.; "A k-ς (Enstrophy) Compressible Turbulence model for Mixing Layer and Wall Bounded Flows," *AIAA paper* 1996-2039, 1996.

[20] Fotia, M.L and Driscoll J.F.; "Experimental Investigation of Ram/Scram-mode Transition Mechanics," *AIAA paper* 2012-5835, 2012, pp. 1-16.

[21] Micka, D.J and Driscoll, J.F; "Dual-Mode Combustion of a Jet in Cross-Flow with Cavity Flameholder," *AIAA paper* 2008-1062, 2008, pp. 1-13.

[22] Chandra Murty, M.S.R., Mishal, R.D. and Chakraborty, D.; "Numerical Simulation of Supersonic Combustion with Parallel Injection of Hydrogen Fuel," *Journal of Defense Science*, Vol. 60, No. 5, 2010, pp. 465-475.

[23] Connaire, M.O., Curran, H.J. Simmie, J.M., Pitz, W.J. and Westbrook, C.K.; "A Comprehensive Modeling Study of Hydrogen Oxidation," *International Journal of Chemical Kinetics*, Vol. 36, No. 11, 2004, pp. 603-622.

[24] Ebrahimi, H. and Gaitonde, D.; "Parametric Study of 3D Hydrocarbon Scramjet Engine with Cavity," *AIAA paper*-200-645, 2007, pp.1-6.

[25] Shapiro, A. H., "The Dynamics and Thermodynamics of Compressible Flow", Wiley, New York, 1975, Chap. 8.

[26] Heiser, W. H., and Pratt, D. T., "Hypersonic Airbreathing Propulsion", AIAA Education Series, AIAA, Reston, VA, 1994, Chap. 6.